Increasing energy efficiency of high-speed parallel robots by using variable stiffness springs and optimal motion generation

Rafael Balderas Hill, Sébastien Briot, Abdelhamid Chriette, Philippe Martinet

Increasing energy efficiency of high-speed parallel robots by using variable stiffness springs and optimal motion generation

Rafael Balderas Hill [†*], Sébastien Briot [‡*], Abdelhamid Chriette [†*], and Philippe Martinet [*§]

[†] Ecole Centrale de Nantes, 44321 Nantes, France
[‡] Centre National de la Recherche Scientifique (CNRS)
[*] Laboratoire des Sciences du Numérique de Nantes (LS2N), UMR CNRS 6004, 44321 Nantes, France
[§] Centre de Recherche Inria Sophia Antipolis, 06902 Sophia Antipolis, France
Email: {Rafael.Balderashill, Sebastien.Briot, Abdelhamid.Chriette}@ls2n.fr, Philippe.Martinet@inria.fr

June 26, 2019

Abstract

The classical approach to decrease the energy consumption of high-speed robots is by lowering the moving elements mass in order to have a lightweight structure. Even if this allows reducing the energy consumed, the lightweight architecture affects the robot stiffness, worsening the accuracy of the mechanism. Recently, variable stiffness actuators (VSAs) have been used in order to reduce the energy consumption of high-speed pick-and-place robots. The idea is to smartly tune online the stiffness of VSA springs so that the robot is put in near a resonance mode, thus considerably decreasing the energy consumption during fast pseudo-periodic pick-and-place motions. However, the serial configuration of springs and motors in the VSA leads to uncontrolled robot deflections at high-speeds and, thus, to a poor positioning accuracy of its end-effector.

In order to avoid these drawbacks and to increase the energy efficiency while ensuring the accuracy, this paper proposes the use of parallel arrangement of variable stiffness springs (VSS) and motors, combined with an energy-based optimal trajectory planner. The VSS are used as energy storage for carrying out the reduction of the energy consumption and their parallel configuration with the motors ensure the load balancing at high-speed without los-ing the accuracy of the robot. Simulations of the suggested approach on a five-bar mechanism are performed and show the increase on energy efficiency.

1 INTRODUCTION

It is well-known that in industrial applications, such as high-speed pick-and-place operations, parallel robots are widely used [1, 2]. Repeatability and accuracy are typically the most important criteria to measure their performance. Nevertheless, the design trends to operate at high speeds are shifting to the design of robots with lightweight architectures [3] in order to decrease the energy consumed by the motors, and measure as well the robot performance based on its energy efficiency [4].

For slow motions, gravity-balancing techniques [5–8] have been proposed in order to compensate the input efforts required to move the links of a pick-and-place robot, and thus to avoid consuming energy. Even if these methods have shown their effectiveness at slow speeds, it is not the case for high-speed operations in which the inertial effects are preponderant. A first solution introduced the series elastic actuators (SEAs) [9] to cope with the energy storage issues. The SEAs are compliant actuators composed by a motor which is linked to a spring in series that serves as energy storage, and whose stiffness is

1

set by the spring constant. SEAs were first used to absorb contact shocks and to reduce the peak forces due to the impacts in bipedal walking robots [10]. The limitation of the SEAs is that the stiffness is fixed and cannot be altered during motion, thus limiting the level of compliance to adapt for different tasks. Therefore, a recent second solution proposed the use of variable stiffness actuators (VSAs) [11–13] to handle with energy storage issues. VSAs consist of a motor which is connected to the output link by a spring in series and whose stiffness is variable and can be controlled. These springs are called Variable Stiffness Springs (VSS) [14]. Such actuators were first introduced for human-robot interaction applications [15], for decreasing contact shocks and for efficiently actuate legged locomotion systems [16, 17]. Recently, they have been used for considerably decreasing the energy consumption of a pick-and-place robot in [18, 19]. Even if the results seem to be impressive, their power consumption models do not consider the energetic losses from the motors that actuate the VSS, thus missing the losses of the full actuation chain. Furthermore, the *serial arrangement of springs and motors* would limit their operational speeds due to uncontrolled robot deflections when performing high-speed tasks.

A novel type of actuation for pick-and-place operations has been presented in [20], where the authors proposed the use of constant stiffness springs in parallel to the motors in order to reduce the energy consumption. The main idea is to place the constant stiffness springs in parallel so that the required torque to move the output load is distributed between the motor and the parallel spring. This is possible since the constant stiffness spring in parallel supplies part of the required input effort to move the output load, thus reducing the energy consumption. Even if the results are impressive, the level of compliance to adapt to fast pseudo-periodic pick-and-place tasks is restricted due to the fixed stiffness.

The use of parallel elastic actuation seems to be a promising solution for increasing the energy efficiency. Therefore, the aim of this paper is to propose a strategy for reducing the energy consumed in high-speed pick-and-place robots by studying the concept of using VSS *in parallel* to the motors, contrary to [18, 19] in which they were mounted in series, as said previously. By placing the VSS in parallel, we will ensure direct power connection between the motor and links of the robot (and thus

to have accuracy at high-speeds), and also to have tunable energy storage through the VSS. Additionally, contrary to what was done in [18, 19], we deal with the minimization of the energetic losses from *the full actuation chain*, i.e., both the parallel robot joints motors and the variable stiffness springs motors, by finding the optimal robot trajectory thanks to an optimization problem.

This paper is divided as follows: Section 2 presents some recalls on the computation of the dynamic model of parallel robots. In addition to that, the dynamic model of parallel robots with VSS is shown. Then, the model of power losses is formulated considering the overall motor drive system. Section 3 shows the optimal problem formulation including the trajectory definition, cost function and decision variables. Section 4 presents the results of the proposed approach on a five-bar mechanism. In order to show the effectiveness of the approach presented in this paper, four cases are analyzed and compared:

1. Nominal case, which consists of the parallel robot without any compliant element, and with a classical fifth-degree polynomial trajectory;

2. Nominal case, with the proposed optimal trajectory planning algorithm;

3. Use of fixed stiffness springs in parallel with the actuated links of the robot, and with optimal motion planner;

4. Use of VSS in parallel with the robot with optimal motion planner.

Finally, the conclusions and future works on this topic are given.

2 PHYSICAL BACKGROUND

The paper aims at providing a strategy for increasing the energy efficiency of high-speed robots based on the concept of parallel VSS, it is thus necessary to make first some recalls on physical preliminaries of parallel robots, elastic actuation and motors modeling.

2.1 Dynamic modeling of parallel robots

Let us briefly recall the dynamic modeling of parallel robots presented in [21]. We will assume a parallel robot
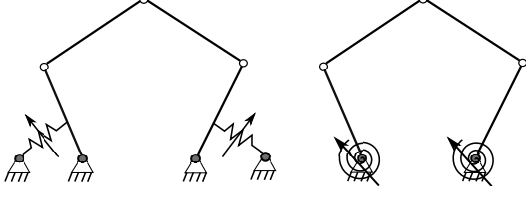
Figure 1: ON THE LEFT, A FIVE-BAR MECHANISM WITH VARIABLE STIFFNESS LINEAR SPRINGS IN PARALLEL ARRANGEMENT WITH THE ACTUATED LINKS IS SHOWN. ON THE RIGHT THE SAME PARALLEL ROBOT WITH VARIABLE STIFFNESS TORSIONAL SPRINGS IS PRESENTED (THE GREY CIRCLES DENOTE THE ACTUATED JOINTS).

composed of n degrees of freedom. The actuation is given by n active joints. The position and velocity of the parallel robot can be described by using:

- $\mathbf{q}$ and $\dot{\mathbf{q}}$ representing the n-dimensional vectors of active joint variables and of active joint velocities, respectively.

- $\mathbf{x}$ and $\dot{\mathbf{x}}$ representing the n-dimensional vectors of platform pose and of its time derivatives, respectively.

The input-output kinematic constraint that relates $\dot{\mathbf{x}}$ with the active joint velocities $\dot{\mathbf{q}}$ is:

$$\mathbf{A}\dot{\mathbf{x}} + \mathbf{B}\dot{\mathbf{q}} = \mathbf{0} \qquad (1)$$

where $\mathbf{A}$ and $\mathbf{B}$ are the $(n \times n)$ parallel and serial kinematic Jacobian matrices, respectively [22]. Then, by using the Lagrange formalism, the dynamic model of the robot can be written as follows:

$$\boldsymbol{\tau} = \boldsymbol{\tau}_{ta} - \mathbf{B}^T \boldsymbol{\lambda} \qquad (2)$$

$$\mathbf{w}_p = \mathbf{A}^T \boldsymbol{\lambda} \qquad (3)$$

where:

- $\boldsymbol{\tau}$ is the n-dimensional vector of the robot input efforts;

- $\boldsymbol{\lambda}$ is the n-dimensional vector of Lagrange multipliers;
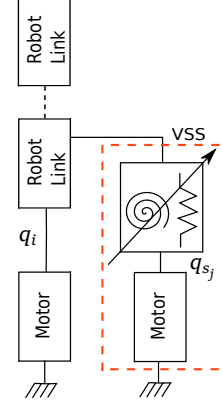

Figure 2: POWER TRANSMISSION SYSTEM OF VARIABLE STIFFNESS SPRINGS IN PARALLEL TO THE MOTORS. q_i AND q_{s_j} REPRESENT THE PARALLEL ROBOT JOINTS AND VARIABLE STIFFNESS JOINTS COORDINATES, RESPECTIVELY, AND $i = 1, ..., n$, $j = 1, ..., n_s$.

- $\boldsymbol{\tau}_{ta}$ and $\mathbf{w}_p$ are the n-dimensional vectors related to the Lagrangian L of the robot defined as the difference between the kinetic energy E and the potential energy U of the system:

$$\boldsymbol{\tau}_{ta} = \frac{\mathrm{d}}{\mathrm{d}t}\left(\frac{\partial L}{\partial \dot{\mathbf{q}}}\right)^T - \left(\frac{\partial L}{\partial \mathbf{q}}\right)^T \qquad (4)$$

$$\mathbf{w}_p = \frac{\mathrm{d}}{\mathrm{d}t}\left(\frac{\partial L}{\partial \dot{\mathbf{x}}}\right)^T - \left(\frac{\partial L}{\partial \mathbf{x}}\right)^T \qquad (5)$$

From equations (2) and (3), considering matrix $\mathbf{A}$ to be full rank, the dynamic model of a parallel robot is obtained:

$$\boldsymbol{\tau} = \boldsymbol{\tau}_{ta} - \mathbf{B}^T \mathbf{A}^{-T} \mathbf{w}_p \qquad (6)$$

which, according to [21], can also be written under the form:

$$\boldsymbol{\tau} = \mathbf{M}\ddot{\mathbf{q}} + \mathbf{h}(\mathbf{q}, \dot{\mathbf{q}}) \qquad (7)$$

where $\mathbf{M}$ is an $(n \times n)$ definite positive matrix of inertia depending on the active joints coordinates $\mathbf{q}$ and platform coordinates $\mathbf{x}$. $\mathbf{h}$ is an n_s-dimensional vector of Coriolis, centrifugal and gravitational effects and its value depends on the active joint coordinates $\mathbf{q}$, and their time derivatives

$\dot{\mathbf{q}}$.

2.2 Modeling of VSS in parallel configuration with the actuated links

Let us consider a parallel robot with VSS in parallel to the actuated links (Fig. 1). According to Fig. 2, the actuation of the VSS is given by n_s active joints. Their position and velocity are given by $\mathbf{q}_s$ and $\dot{\mathbf{q}}_s$ representing the n_s-dimensional vectors of variable stiffness joint variables and of variable stiffness joint velocities, respectively. By considering the effects of the elastic deformation of the springs with their force/displacement relations, the dynamics in (7), become:

$$\boldsymbol{\tau} = \mathbf{M}\ddot{\mathbf{q}} + \mathbf{h}(\mathbf{q},\dot{\mathbf{q}}) + \boldsymbol{\tau}_s \qquad (8)$$

where $\boldsymbol{\tau}_s$ is the n_s-dimensional vector of elastic torques associated to the VSS coupled to the robot in parallel:

$$\boldsymbol{\tau}_s = \mathbf{K}(\mathbf{q} - \mathbf{q}_s) \qquad (9)$$

where $\mathbf{K}$ is the $(n_s \times n_s)$ stiffness matrix, and the dynamics of the VSS is expressed by:

$$\boldsymbol{\tau}_{vss} = \mathbf{M}_s\ddot{\mathbf{q}}_s + \mathbf{h}_s(\mathbf{q}_s,\dot{\mathbf{q}}_s) - \boldsymbol{\tau}_s \qquad (10)$$

where $\mathbf{M}_s$ is an $(n_s \times n_s)$ definite positive matrix of inertia depending on the variable stiffness joints coordinates $\mathbf{q}_s$, and $\mathbf{h}_s$ is an n_s-dimensional vector of Coriolis, centrifugal and gravitational effects and its value depends on the variable stiffness joints coordinates $\mathbf{q}_s$ and their time derivatives $\dot{\mathbf{q}}_s$.

2.3 Power consumption model of the full actuation chain

In order to study the energy consumed by the motors during their different operation modes, several energy consumption models have been formulated, such as in [19]. For this work we consider direct-drive three phase brushless motors to actuate the joints of the parallel robot and the variable stiffness joints, therefore avoiding energetic losses due to gearboxes. The electromechanical schematics of such motor drive systems vary from manufacturer to manufacturer depending on the type of driver for energizing each phase of the brushless motor. However, five sections can be identified in their electromechanical sys-

tem: (i) three phase rectification, (ii) braking, (iii) six-transistor-commutable bridge, (iv) the three phase brushless motor, and (v) mechanical coupling between motor and drive shaft (for further details on electromechanical systems and power electronics the reader can refer to [23]). Thus, to define the energy consumption model of such brushless motors, five types of power losses are classified:

- **Resistive losses**: These are heat losses that occur when current flows through the resistances of each phase of the brushless motors and the braking resistances. The mathematical expression is given by:

$$P_{motor} = R_{phase}I^2 \qquad (11)$$

$$P_{brake} = R_{brake}I^2 \qquad (12)$$

  where I is the line-to-line current between each phase of the motor, and R_{phase} and R_{brake} are electrical resistances.

- **Damping losses**: These are mechanical losses due to the mechanical coupling between the motor and drive shaft modeled by:

$$P_{damp} = B\dot{q}_k^2 \qquad (13)$$

  where B is the damping coefficient and $\dot{q}_k$ is the velocity of the kth motor axis, where $k = 1, ..., (n + n_s)$.

- **Conduction losses**: The conduction losses are electrical losses due to the current flow through the transistors and diodes occurring in the three phase rectification and the six-transistor-commutable bridge. They are modeled as follows:

$$P_{cond} = \underbrace{u_{ce}I_{c_{av}} + r_cI_{c_{rms}}^2}_{transistors} + \underbrace{u_DI_{D_{av}} + r_DI_{D_{rms}}^2}_{diodes} \qquad (14)$$

  where u_{ce} is the collector-to-emitter voltage and $I_{c_{av}}$ is the collector current, r_c is the on-state resistance and $I_{c_{rms}}$ is the RMS value of the collector current. u_D is the diode forward voltage and $I_{D_{av}}$ is the diode current, r_D is the on-state resistance and $I_{D_{rms}}$ is the RMS value of the diode current.

- **Switching losses**: These losses occur due to the continuous switching in the six-transistor-commutable

bridge of the motor driver when energizing each phase of the motor. The relationship is given by:

$$P_{switch} = \underbrace{u_{ce}I_{c_{av}}f_{sw}}_{transistors} + \underbrace{u_D I_{D_{av}}f_{sw}}_{diodes} \qquad (15)$$

where f_{sw} is the switching frequency from the six-transistor-commutable bridge.

- **Rectification losses**: These are electrical losses generated from the power supply of three phase rectification modeled as follows:

$$P_{rectifier} = u_{DR}I_{DR_{av}} + r_{DR}I_{DR_{rms}}^2 \qquad (16)$$

where u_{DR} is the diode rectifier forward voltage and $I_{DR_{av}}$ is the diode rectifier current, r_{DR} is an on-state resistance and $I_{DR_{rms}}$ is the RMS value of the diode rectifier current.

It should be mentioned that the currents $I_{c_{av}}$, $I_{c_{rms}}$, $I_{D_{av}}$, $I_{D_{rms}}$, $I_{DR_{av}}$ and $I_{DR_{rms}}$, associated to the conduction, switching and rectification losses due to the diodes and transistors, are functions of the line-to-line currents I of the motor and thus, by using the model of the brushless motor in [24], and functions of the motor electromagnetive torque $\boldsymbol{\tau}_e$, and input torque $\boldsymbol{\tau}$. The expressions linking all these variables are not given here due to page limitations, but can be found in [25].

Finally, by grouping the aforementioned power losses, the following model of losses results:

$$\begin{aligned} P_{losses} = P_{motor} + P_{brake} + P_{damp} \\ P_{cond} + P_{switch} + P_{rectifier} \end{aligned} \qquad (17)$$

By investigating the mathematical formulations (modeling the dynamics of parallel robots and the power losses of their motor drive systems) it is not evident to see how to minimize the energy consumption. For this reason, it is thus necessary to find a strategy to exploit the power consumption model in order to minimize the power losses during the motion.

3 Optimal problem formulation for minimizing the energetic losses on parallel robots

In order to cope with an optimal approach to minimize the energetic losses presented in section 2, an optimal trajectory planning algorithm is designed. The main idea is to define a motion generator such that the energetic losses, computed from numerical integration of (17), are minimized, i.e. to find an optimal trajectory $\mathbf{q}(t)$ (or $\mathbf{x}(t)$ if expressed in Cartesian space) and optimal spring coordinates $\mathbf{q}_s(t)$ that minimizes the energetic losses during the motion.

For a pick-and-place manipulator, there is no restriction for the robot on how to go from the initial to the final positions, except eventual collisions within the robot links, external environment or singularity loci. That is why, similar to what it was done in [26], our trajectory planning algorithm finds a path sequence of via points (intermediate points) between the initial and final positions (Fig. 3 and 4), which are then interconnected by the motion profiles defined thereafter.

Our proposed energy-based optimal trajectory planner is thus an algorithm which minimizes an objective function that computes the energy consumed during the motion by finding optimal sequence of via points between initial and final robot positions. In order to do so, we first need to define a trajectory planner that fully exploits the dynamic performances of the modified high-speed parallel robot so that the cost function based on the power losses can be minimum. It is described thereafter.

3.1 Trajectory definition

In order to develop the motion planners, we decided to denote as M_s the total number of via points along the variable stiffness joints trajectory and as M the total number of via points along the parallel robot joints trajectory. The total duration of the trajectory is denoted as t_f and we impose the duration of the motion between two successive via-points to be equal to $\delta t_s = t_f/(M_s + 1)$ for the variable stiffness joints trajectory and to $\delta t = t_f/(M+1)$ for the robot joint trajectory.

5

3.1.1 Variable stiffness joints trajectories

Different to what it has been done in [11, 13], in which the authors proposed to find motion profiles for the stiffness rather than the variable stiffness joints, this paper generates directly the joint trajectories for the motors that actuate the VSS. This avoids to handle further computations for calculating the stiffness and allows the use of a classical position controller, avoiding the issue of measuring the stiffness in the feedback. In order to generate the variable stiffness joint motion planner let us express $\mathbf{q}_s$ from (8) as follows:

$$\mathbf{q}_s = -\mathbf{K}^{-1}(\boldsymbol{\tau} - \mathbf{M}\ddot{\mathbf{q}} - \mathbf{h}(\mathbf{q}, \dot{\mathbf{q}})) + \mathbf{q} \qquad (18)$$

Based on expression (18), it is possible to observe that the variable stiffness joint dynamics in (10), and therefore the optimal spring stiffness, is dependent, not only on $\mathbf{q}_s$ and its time derivatives $\dot{\mathbf{q}}_s$ and $\ddot{\mathbf{q}}_s$ but also on the configuration of the parallel robot joints $\mathbf{q}$, and their velocities $\dot{\mathbf{q}}$ and accelerations $\ddot{\mathbf{q}}$.

We build the variable stiffness joint motion planner as follows. For the jth component of the vector $\mathbf{q}_s$ denoted as q_{sj}, let us consider a sequence of two successive via-points $q_{sj_k} = q_{sj}(t_{s,k})$ and $q_{sj_{k+1}} = q_{sj}(t_{s,k+1})$ on the time interval $t \in [t_{s,k}, t_{s,k+1}]$ with $t_{s,k} = t_0 + k\,\delta t_s$ ($k = 0, ..., M_s$) and $t_{s,k+1} = t_{s,k} + \delta t_s$ (one of the via-points can be replaced by the initial or final point of the trajectory). Taking advantage of model (18), we connect the via-point q_{sj_k} and $q_{sj_{k+1}}$ (Fig. 4) thanks to the following expression defined by means of several polynomials, valuable on the time interval $t \in [t_{s,k}, t_{s,k+1}]$:

$$q_{sj}(t) = p_{1j}^{(k)}(q_j(t)) + p_{2j}^{(k)}(\dot{q}_j(t)) + p_{3j}^{(k)}(\ddot{q}_j(t)) + p_{4j}^{(k)}(t) \tag{19}$$

where $p_{1j}^{(k)}(q_j(t))$ is a polynomial of $q_j(t)$, $p_{2j}^{(k)}(\dot{q}_j(t))$ is a polynomial of $\dot{q}_j(t)$, $p_{3j}^{(k)}(\ddot{q}_j(t))$ is a polynomial of $\ddot{q}_j(t)$, and finally $p_{4j}^{(k)}(t)$ is a polynomial of time that is used to model the effects of $\boldsymbol{\tau}$ on q_{sj}. The motion profile used for $q_j(t)$ will be defined later in Section 3.1.2.

In order to obtain the explicit form of each polynomial, we follow a heuristic approach of experimentally testing different functions until obtaining the best polynomial form based on the energy consumed during the motion. After trials and errors, we found the best results
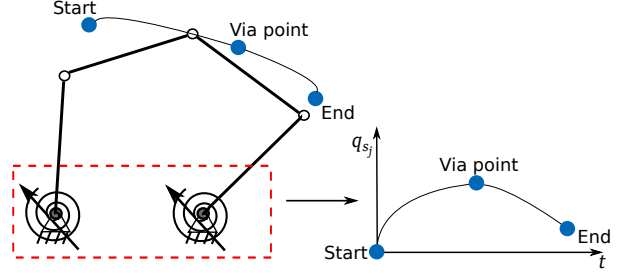

Figure 3: SCHEMATIC OF VIA-POINT TRAJECTORY FOR PARALLEL ROBOT AND VARIABLE STIFFNESS JOINTS.
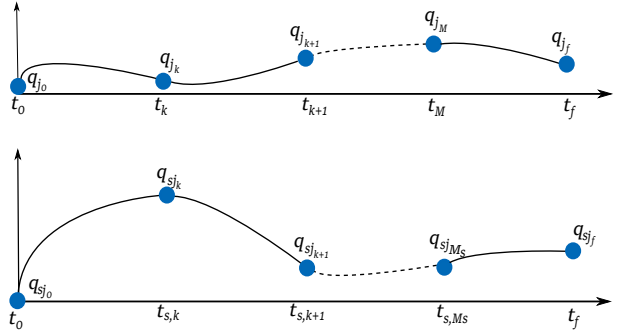

Figure 4: ON THE TOP A VIA-POINT TRAJECTORY FOR THE PARALLEL ROBOT JOINTS WITH M VIA-POINTS. ON THE BOTTOM A VIA-POINT TRAJECTORY FOR THE VARIABLE STIFFNESS JOINT MOTION PLANNER WITH M_S VIA-POINTS.

when:

$$p_{1j}^{(k)}(q_j(t)) = 0, \ p_{2j}^{(k)}(\dot{q}_j(t)) = 0 \qquad (20)$$

$$p_{3j}^{(k)}(\ddot{q}_j(t)) = K_{jk}\ddot{q}_j^3 + K_{j(k+1)}\ddot{q}_j^2 + K_{j(k+2)}\ddot{q}_j + K_{j(k+3)} \tag{21}$$

$$p_{4j}^{(k)}(t) = (q_{sj_{k+1}} - q_{sj_k})(\alpha_{0sjk} + \alpha_{1sjk}t + \alpha_{2sjk}t^2 + \\ \alpha_{3sjk}t^3 + \alpha_{4sjk}t^4 + \alpha_{5sjk}t^5) \tag{22}$$

Parameters $(K_{jk}, ..., K_{j(k+3)})$ are set as decision vari-

ables of the optimization problem, as well as the parameters q_{sj_k}, v_{sj_k} and a_{sj_k} for $k = 1, ..., M_s$. Note that, in our case, in order to simplify the resolution of the optimization problem, we decide to use the same values of the parameters $(K_{jk}, ..., K_{j(k+3)})$ for any segment between two consecutive via-points.

The boundary and continuity conditions between each portion of motion are defined as follows:

$$
\begin{cases}
q_{sj}(t_{s,k}) = q_{sj_k} \text{ and } q_{sj}(t_{s,k+1}) = q_{sj_{k+1}} \\
\dot{q}_{sj}(t_{s,k}) = v_{sj_k} \text{ and } \dot{q}_{sj}(t_{s,k+1}) = v_{sj_{k+1}} \\
\ddot{q}_{sj}(t_{s,k}) = a_{sj_k} \text{ and } \ddot{q}_{sj}(t_{s,k+1}) = a_{sj_{k+1}} \\
q_{sj}(t_0) = q_{sj_0} \text{ and } q_{sj}(t_f) = q_{sj_f} \\
\dot{q}_{sj}(t_0) = 0 \text{ and } \dot{q}_{sj}(t_f) = 0 \\
\ddot{q}_{sj}(t_0) = 0 \text{ and } \ddot{q}_{sj}(t_f) = 0
\end{cases}
\tag{23}
$$

where v_{sj_k} and a_{sj_k} ($v_{sj_{k+1}}$ and $a_{sj_{k+1}}$, resp.) represent the velocity and acceleration of the variable stiffness joint j at via-point k ($k+1$, resp.). For a given set of parameters v_{sj_k}, $v_{sj_{k+1}}$, a_{sj_k}, $a_{sj_{k+1}}$, $(K_{jk}, ..., K_{j(k+3)})$ and robot joint trajectory $q_j(t)$, the boundary and continuity conditions (23) are used in order to compute the coefficients α_{lsjk} in (22).

3.1.2 Parallel robot trajectory generation

Since our motion planner for $\mathbf{q}_s$ is a function of $\ddot{\mathbf{q}}$ and because Eq. (10) depends on $\ddot{\mathbf{q}}_s$, it is necessary to constrain jerks and the derivative of the jerks of $\mathbf{q}$. For the jth component of the vector $\mathbf{q}$ denoted as q_j, let us consider a sequence of two successive via-points $q_{j_k} = q_j(t_k)$ and $q_{j_{k+1}} = q_j(t_{k+1})$ on the time interval $t \in [t_k, t_{k+1}]$ with $t_k = t_0 + k\,\delta t$ ($k = 0, ..., M$) and $t_{k+1} = t_k + \delta t$ (one of the via-points can be the initial or final point of the trajectory). The trajectory for q_j between via-points q_{j_k} and $q_{j_{k+1}}$ is thus defined by using ninth-degree time-dependent polynomials which can fix the position, velocities, accelerations, jerks and derivatives of the jerks at both via-points. The expression of the polynomial on the time interval $t \in [t_k, t_{k+1}]$ is given by:

$$
q_j(t) = (q_{j_{k+1}} - q_{j_k})(\alpha_{0jk} + \alpha_{1jk}t + \alpha_{2jk}t^2 + \alpha_{3jk}t^3 + \\
\alpha_{4jk}t^4 + \alpha_{5jk}t^5 + \alpha_{6jk}t^6 + \alpha_{7jk}t^7 + \alpha_{8jk}t^8 + \alpha_{9jk}t^9)
\tag{24}
$$

The boundary and continuity conditions are defined as follows:

$$
\begin{cases}
q_j(t_k) = q_{j_k} \text{ and } q_j(t_{k+1}) = q_{j_{k+1}} \\
\dot{q}_j(t_k) = v_{j_k} \text{ and } \dot{q}_j(t_{k+1}) = v_{j_{k+1}} \\
\ddot{q}_j(t_k) = a_{j_k} \text{ and } \ddot{q}_j(t_{k+1}) = a_{j_{k+1}} \\
q_j(t_0) = q_{j_0} \text{ and } q_j(t_f) = q_{j_f} \\
\dot{q}_j(t_0) = 0 \text{ and } \dot{q}_j(t_f) = 0 \\
\ddot{q}_j(t_0) = 0 \text{ and } \ddot{q}_j(t_f) = 0
\end{cases}
\tag{25}
$$

and $q_j^{[3]}(t_k) = 0$ and $q_k^{[4]}(t_k) = 0$ at any via-point or at the initial and final points. In (25), v_{j_k} and a_{j_k} ($v_{j_{k+1}}$ and $a_{j_{k+1}}$, resp.) represent the velocity and acceleration of the robot joint joint j at via-point k ($k+1$, resp.). For given values of parameters v_{j_k}, $v_{j_{k+1}}$, a_{j_k}, $a_{j_{k+1}}$, the boundary and continuity conditions (25) are used in order to compute the coefficients α_{ljk} in (24).

Parameters q_{j_k}, v_{j_k} and a_{j_k} for $k = 1, ..., M$ are set as decision variables of the optimization problem.

3.2 Optimization Problem Formulation: Cost function and decision variables

The optimization problem aims to minimize the energetic losses of the modified parallel robot that considers the full actuation chain, taking into account physical constraints of the robot and the motors. The cost function of the optimization problem corresponds to the power losses of the motors that actuate the parallel robot joints and the variable stiffness joints since the manipulator must be as energy efficient as possible. The cost function for the optimizing process is thus defined as follows:

$$
J = \int_0^{t_f} \sum_{k=1}^{n+n_s} P_{losses_k} dt
\tag{26}
$$

where P_{losses_k} represents the power losses of the kth motor of the full actuation chain from expression (17).

Based on the description of the trajectory planner in the previous sections, the decision variable vector of the optimization problem, denoted as $\mathbf{x_{DecVar}}$, contains all aforementioned parameters q_{j_k}, q_{sj_k}, v_{j_k}, v_{sj_k}, a_{j_k}, a_{sj_k} and $(K_{jk}, ..., K_{j(k+3)})$.

The optimal trajectory through via-points problem aims at finding the decision variable vector $\mathbf{x_{DecVar}}$ that minimizes the power losses of the $(n + n_s)$ motors while re-

specting physical constraints, such as motor limits and collisions. In this paper, we handle the collision avoidance of virtual obstacles, which represents singularity loci of the parallel robot. This to prevent of finding via-points in the neighborhood of the parallel robot singularities.

The optimization problem was solved by means of MATLAB $fmincon$ function and it is formulated as follows:

$$
\begin{aligned}
\text{minimize} \quad & J \\
\text{over} \quad & \mathbf{x_{DecVar}} \\
\text{subject to} \quad & |\tau_{e_k}| \leq \tau_{e_{max}} \\
& |\kappa| < \epsilon
\end{aligned}
\tag{27}
$$

where τ_{e_k} is the electromagnetive torque of the kth motor and κ represents the condition of proximity to the singularity with ϵ denoting a threshold tuned experimentally. For a detailed overview on singularities of parallel robots the reader can refer to [27, 28].

4 CASE STUDY

4.1 Five-bar mechanism with variable parallel elastic actuation

The proposed optimization approach for increasing the energy efficiency was validated in a five-bar mechanism with variable stiffness torsional springs in parallel, as shown in Fig. 5. The actuation of the parallel robot is provided by $\mathbf{q} = [q_{11}, q_{21}]^T$. The vector of passive joints is given by $\mathbf{q}_d = [q_{12}, q_{22}, q_{13}]^T$. The vector of moving platform pose is given by $\mathbf{x} = [x, y]^T$. a is the distance between the actuated joints. All link lengths l are identical. The actuation for the variable stiffness joints is given by $\mathbf{q}_s = [q_{s1}, q_{s2}]^T$.

The numerical values of the five-bar mechanism geometric and dynamic parameters were defined according to a real parallel robot called RobEcolo in [29] [30], and have the following values:

- inertia of the two proximal links $zz_{11} = 0.133$ kg/m^2 and $zz_{21} = 0.122$ kg/m^2;

- Coulomb friction terms of the actuated joints $f_{s1} = 0.659$ Nm and $f_{s1} = 0.225$ Nm;

- end-effector mass $m = 1.84$ kg;

- inertias of the couplings between the motors and springs $J_1 = J_2 = 0.0051$ kg/m^2;

- stiffness constants of the springs $k_{11} = k_{21} = 4$ Nm/rad;

- link lengths of the two proximal links $l_1 = l_2 = 0.28$ m;

- link lengths of the two distal links $l_3 = l_4 = 0.4$ m;

- distance between the axes of the actuated links $a = 0.250$ m.

The motor parameters used to examine the energetic performance with the proposed approach were defined according to the motor specifications found in [31] by the following values:

- electrical resistances $R_{phase} = 0.2$ Ω, $R_{brake} = 18$ Ω;

- damping coefficient $B = 0.005$ Nm/s;

- on-state resistances $r_c = r_D = r_{DR} = 0.003$ Ω;

- forward and collector-to-emitter voltages $u_D = u_{DR} = u_{ce} = 0.8$ V;

- switching frequency $f_{sw} = 20$ KHz.

The algorithm validation was performed by using the dynamic model of the real parallel robot called RobEcolo [29] [30], which is a wooden five-bar mechanism whose dynamic model is given by the following equations:

$$
\boldsymbol{\tau} = \mathbf{ZZ}\ddot{\mathbf{q}} + \mathbf{B}^T\boldsymbol{\lambda} + \begin{bmatrix} f_{s_1}\text{sign}(\dot{q}_1) \\ f_{s_2}\text{sign}(\dot{q}_2) \end{bmatrix} + \boldsymbol{\tau}_s \tag{28}
$$

$$
\mathbf{w}_p = \mathbf{A}^T\boldsymbol{\lambda} = m\ddot{\mathbf{x}} \tag{29}
$$

where $\mathbf{A}$ and $\mathbf{B}$ are computed from the input-output kinematic constraint relation (1), and $\boldsymbol{\tau}_s$ is calculated from (9). $\mathbf{ZZ} = \text{diag}(zz_{11}, zz_{21})$, with zz_{11} and zz_{21} representing the inertia of the two proximal links, and $\mathbf{K} = \text{diag}(k_{11}, k_{21})$, with k_{11}, k_{21} being the springs constants. Finally, the VSS dynamics from (10) is given by:

$$
\boldsymbol{\tau}_{vss} = \begin{bmatrix} J_1 & 0 \\ 0 & J_2 \end{bmatrix} \begin{bmatrix} \ddot{q}_{s1} \\ \ddot{q}_{s2} \end{bmatrix} - \underbrace{\begin{bmatrix} k_{11} & 0 \\ 0 & k_{21} \end{bmatrix} \begin{bmatrix} (q_{11} - q_{s1}) \\ (q_{21} - q_{s2}) \end{bmatrix}}_{\boldsymbol{\tau}_s} \tag{30}
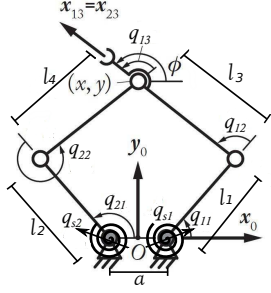$$

Figure 5: FIVE-BAR MECHANISM PARAMETERIZA-TION WITH TWO ACTUATED JOINTS q_{11} AND q_{21}, AND THREE PASSIVE JOINTS q_{12}, q_{22} AND q_{13}. THE VARIABLE STIFFNESS TORSIONAL SPRINGS ARE LOCATED IN PARALLEL TO THE TWO ACTUATED JOINTS DEFINED BY q_{s1} AND q_{s2}.

4.2 Results and comparative energetic analysis on three cases: nominal, constant stiffness and variable stiffness actuation

In order to validate the theoretical formulations, the optimization algorithm is tested by defining multiple desired points in the workspace of the five-bar mechanism as shown in Fig. 6. The aim is to go multiple times to these points by finding the appropriated optimal decision variable vector $\mathbf{x_{DecVar}}$ that minimizes the energetic losses of the full actuation chain. The sections of trajectories are defined between the points given by: $A = [0.25, 0.3], B = [0, 0.4], C = [0.2, 0.5], D = [0, 0.45], E = [0.2, 0.4], F = [0, 0.5], G = [0.2, 0.35]$. The sequence of the trajectory is defined at Fig. 6. For showing the effectiveness of the proposed approach, the input torques and the energy consumption of four different types of actuation are analyzed: (i) Nominal actuation, in which there is no elastic element attached at each joint, and a fifth-degree polynomial trajectory is used between each set of two successive points; (ii) nominal actuation with optimized trajectory; (iii) actuation with fixed stiffness springs in parallel with each joint of the robot, with spring constants k_{11} and k_{21} defined according to section 4.1, and with optimized trajectory; (iv) actuation with

VSS in parallel with each actuated link of the robot and with optimized trajectory. Figures 7 and 8 show the input torques computed for the four types of actuation in the parallel robot joints along the multiple trajectories from the sequence in Fig. 6 with travel times of 0.2 s between each desired set of two points. It can be seen that in both parallel robot actuated joints, the input torques are reduced by using springs, with fixed stiffness and then with variable stiffness, being the latter the type of actuation with major gain in reduction of input efforts. The torques shown in Fig. 9 correspond to the input torques of the variable stiffness joints. As compared to the parallel robot joint torque magnitudes, the variable stiffness joint torques do not have a major impact on input efforts. Then, Fig. 10 shows the energetic losses from the power consumption model (17) for the four types of actuation. It can be seen that by using VSS, it is possible to reduce the energy up to 48 % with respect to the nominal case with classical fifth-degree polynomial trajectory. It should be mentioned that this result is far from the gain in energy efficiency of 90 % shown in [19], but this is due to the fact that, in our work, we did not neglect any losses in the actuation chain including the VSS and the motor driver, which was not the case at all in [19].

In addition to that, Fig. 11 shows the energy consumption reduction achieved by using VSS for different pick-and-place travel times between the same points. It can be seen that our algorithm has better performance when performing the most high-speed tasks. In Fig. 12, the influence of modifying the number of via-points for the parallel robot and variable stiffness joints is shown. It is observed that the major reduction occurs when the number of via-points is set to two for both the parallel robot joints and variable stiffness joints. This is due to the fact that increasing the number of via-points and having fast pick-and-place travel times complexified the resolution of the optimization algorithm and made it converged towards local minima. Finally, Fig. 13 shows the energy reduction separately for each identified power loss presented in section 2.3. It can be seen that the major reduction occurs on the resistive losses, which is expected since they are affected by the squared of the electric currents, which are functions of the electromagnetic torques, included as a contraint in the optimization problem.
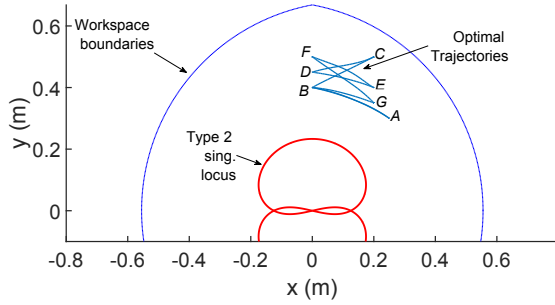
Figure 6: MULTIPLE OPTIMAL TRAJECTORIES FOR THE SEQUENCE: $A \rightarrow B \rightarrow C \rightarrow D \rightarrow E \rightarrow F \rightarrow G \rightarrow B \rightarrow A$, WITH TRAVEL TIMES OF 0.2 s BETWEEN DESIRED POINTS.
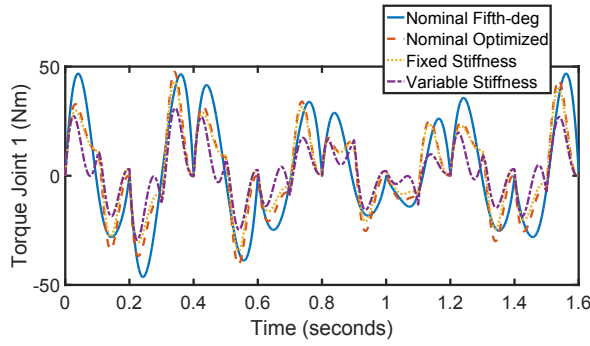

Figure 7: INPUT TORQUES FOR THE FIRST JOINT OF THE PARALLEL ROBOT FOR THE FOUR CASES: NOMINAL FIFTH-DEGREE POLYNOMIAL, NOMINAL WITH OPTIMIZED TRAJECTORY, FIXED STIFFNESS AND VARIABLE STIFFNESS, 0.2 s AS PICK-AND-PLACE TRAVEL TIME BETWEEN DESIRED POINTS.
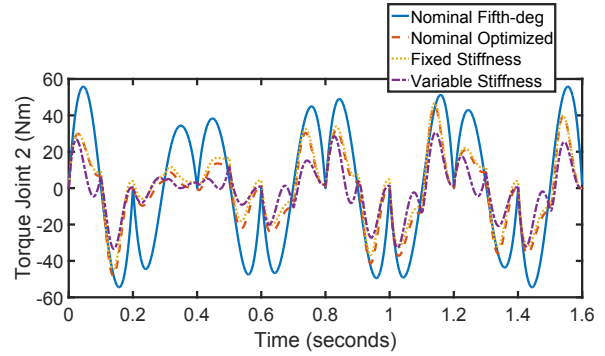

Figure 8: INPUT TORQUES FOR THE SECOND JOINT OF THE PARALLEL ROBOT FOR THE FOUR CASES: NOMINAL FIFTH-DEGREE POLYNOMIAL, NOMINAL WITH OPTIMIZED TRAJECTORY, FIXED STIFFNESS AND VARIABLE STIFFNESS, 0.2 s AS PICK-AND-PLACE TRAVEL TIME BETWEEN DESIRED POINTS.
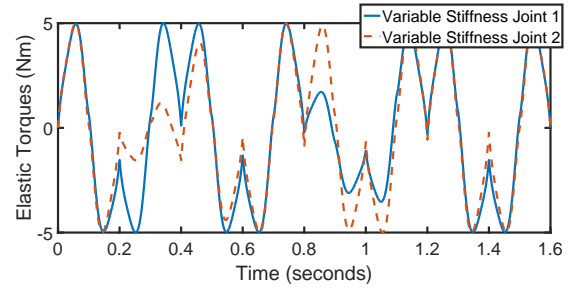

Figure 9: INPUT TORQUES FOR THE JOINTS OF VARIABLE STIFFNESS, 0.2 s AS PICK-AND-PLACE TRAVEL TIME BETWEEN DESIRED POINTS.

5 CONCLUSIONS

This paper proposes a new approach to increase the energy efficiency of high-speed pick-and-place parallel robots by placing variable stiffness springs in parallel with the motors. An analysis of the energetic losses of the full actuation chain provided a cost function which is used in an optimal problem formulation in order to minimize the power losses. Then, specific trajectories for the parallel robot joints and for the variable stiffness joints were de-

veloped avoiding to have a nonlinear force/displacement relation for the elastic torques. Simulations led to the successful increasing of energy efficiency with multiple-point trajectories on a five-bar mechanism for four cases: nominal with a classical fifth-degree polynomial, nominal with optimized trajectory, use of fixed stiffness and variable stiffness springs. Results show that the reduction of energy consumption can reach up to 48 % when using VSS. Next work on this subject includes experimental validation of our approach and the design of an alternative optimization strategy in order to tune the spring coordi-
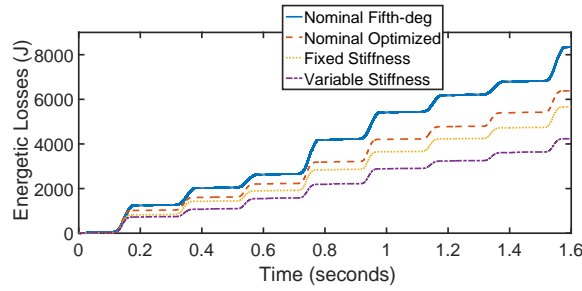
Figure 10: ENERGETIC LOSSES FOR THE FOUR CASES ANALYZED: NOMINAL FIFTH-DEGREE POLYNOMIAL, NOMINAL WITH OPTIMIZED TRAJECTORY, FIXED STIFFNESS AND VARIABLE STIFFNESS, 0.2 s AS PICK-AND-PLACE TRAVEL TIME BETWEEN DESIRED POINTS.
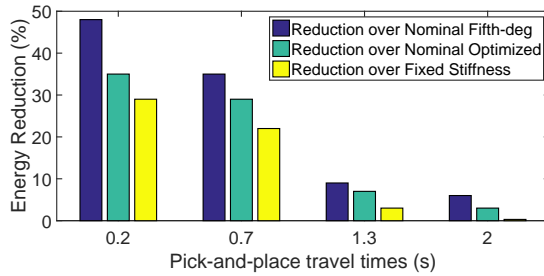

Figure 11: REDUCTION OF ENERGY CONSUMPTION FOR DIFFERENT PICK-AND-PLACE TRAVEL TIMES BETWEEN DESIRED POINTS WHEN USING VSA.
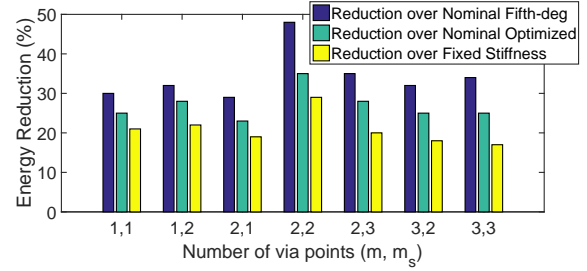

Figure 12: REDUCTION OF ENERGY CONSUMPTION FOR DIFFERENT NUMBER OF VIA-POINTS WITH 0.2 s AS PICK-AND-PLACE TRAVEL TIME BETWEEN DESIRED POINTS.
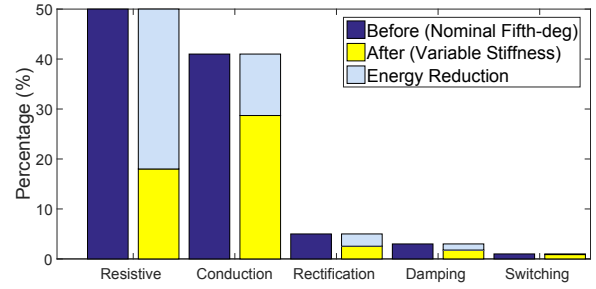

Figure 13: ENERGY REDUCTION FOR EACH IDENTIFIED POWER LOSS.

nates online, avoiding the pre-computation of the motion planners.

Acknowledgment

References

[1] Krut, S., Nabat, V., Company, O., Pierrot, F., 2004. A high-speed parallel robot for scara motions. In Proc. of International Conference on Robotics and Automation, New Orleans, USA, pp. 4109-4115.

[2] Angeles, J., Caro, S., Khan, W., Morozov, A., 2006. Kinetostatic design of an innovative schoenflies-motion generator. In Proc. of IMechE Part C: Journal of Mechanical Engineering Science, *220* (7), pp. 935-943.

[3] Clavel R., 1990. Device for the movement and positioning of an element in space. US Patent 4 976 582, December 11.

[4] Brossog, M., Bornschlegl, M., Franke, J., 2015. Reducing the energy consumption of industrial robots in manufacturing systems. International Journal of Advanced Manufacturing Technology, Vol. 78 Issue 5-8, pp. 1315-1328.

[5] Baradat, C., Arakelian, V., Briot, S., and Gugan, S., 2008. Design and Prototyping of a New Balancing Mechanism for Spatial Parallel Manipulators. ASME, Journal of Mechanical Design, *130*(7).

[6] Briot, S., and Arakelian, V., 2015. A New Energy-free Gravity-compensation Adaptive System for Balancing of 4-DOF Robot Manipulators with Variable Payloads. In Proc. of the 14th International Federation for the Promotion of Mechanism and Machine Science World Congress (2015 IFToMM World Congress), Taipei, Taiwan.

[7] Agrawal, S. K., and Fattah, A., 2004. Reactionless Space and Ground Robots: Novel Designs and Concept Studies. Mech. Mach. Theory, *39*, pp. 25-40.

[8] Wang, J., and Gosselin, C. M., 1999. Static Balancing of Spatial Three-Degree-of-Freedom Parallel Mechanisms. Mech. Mach. Theory, *34*, pp. 437-452.

[9] Pratt, G. A., and Williamson, M. M, 1995. Series elastic actuators. In Proc. of the 1995 IEEE/RSJ International Conference on Intelligent Robots and Systems, Pittsburgh, PA, pp. 399 - 406.

[10] Pratt, J. E., Chee, M. C., Torres, A., Dilworth, P., and Pratt, G. A., 2001. Virtual model control: an intuitive approach for bipedal locomotion. International Journal of Robotics Research, *20*(2), pp. 129-143.

[11] Van Ham, R., Thomas, S., Vanderborght, B., Hollander, K., Lefeber, D., 2009. Compliant actuator designs: review of actuators with passive adjustable compliance/controllable stiffness for robotic applications, IEEE Robotics and Automation Magazine, *16*(3), pp. 81-94.

[12] Vanderborght, B., Albu-Schaeffer, A., Bicchi, A., Burdet, E., Caldwell, D., Carloni, R., Catalano, M., Ganesh, G., Garabini, M., Grioli, G., Haddadin, S., Jafari, A., Laffranchi, M., Lefeber, D., Petit, F., Stramigioli, S., Grebenstein, M., Tsagarakis, N., Van Damme, M., Van Ham, R., Visser, L., Wolf S., 2012. Variable impedance actuators: moving the robots of tomorrow. In: IEEE/RSJ International Conference on Intelligent Robots and Systems, IROS 2012, Vilamoura, Algarve (Portugal).

[13] Wolf, S., Grioli, G., Eiberg, O., Friedl, W., Grebenstein, M., Catalano, M., Lefeber, D., Stramigioli, S., Tsagarakis, N., Van Damme, M., Van Ham, R., Vanderborfht, B., Visser, L.C., Bicchi, A., Albu-Schaeffer, A., 2016. Variable stiffness actuators: Review on design and components, IEEE/ASM Transactions on Mechatronics, *21*(5), pp. 2418-2430.

[14] Hollander, K., and Sugar, T., 2004. Concepts for compliant actuation in wearable robotic systems. In Proc. of the US-Korea Conference on Science, Technology and Entrepreneurship (UKC04), *128*, pp. 644-650.

[15] Tsagarakis, N., Laffranchi, M., Vanderborght, B., Caldwell D., 2009. A compact soft actuator unit for small scale human friendly robots. In: IEEE Int. Conf. on Robotics and Automation, Kobe, Japan, ICRA 2009, pp. 4356-4362.

[16] Van Ham, R., Vanderborght, B., Van Damme, M., Verrelst, B., Lefeber D., 2007. MACCEPA, the mechanically adjustable compliance and controllable equilibrium position actuator: design and implementation in a biped robot. Robotics and Autonomous Systems, *55*(7), pp. 761-768.

[17] Vanderborght, B., Van Ham, R., Verrelst, B., Van Damme, M., Lefeber D., 2008. Overview of the lucy project: dynamic stabilization of a biped powered by pneumatic artificial muscles. Advanced Robotics, *22*(25), pp. 1027-1051.

[18] Uemura, M., and Kawamura, S., 2009. Resonance-based motion control method for multi-joint robot through combining stiffness adaptation and iterative learning control. In IEEE International Conference on Robotics and Automation, Kobe, Japan, pp. 1543-1548.

[19] Goya, H., Matsusaka, K., Uemura, M., Nishioka, Y., and Kawamura S., 2012. Realization of high-energy efficient pick-and-place tasks of scara robots by resonance. In IEEE/RSJ International conference on Intelligent Robots and Systems, IROS 2012, pp. 2730-2735, Vilamoura, Algarve (Portugal).

[20] Barreto, J.P., Schöler, F.J.-F., and Corves, B., 2017. The concept of natural motion for pick and place operations. In: New advances in mechanisms, mechanical transmissions and robotics. Springer, pp. 89-98.

[21] Briot, S., and Khalil, W., 2015. Dynamics of Parallel Robots: From Rigid Bodies to Flexible Elements. Springer. ISBN: 978-3-319-19788-3.

[22] Merlet, J-P., 2006. Parallel Robots. Springer. ISBN 978-1-4020-4133-4.

[23] Chapman, S. J., 1991. Electric Machinery Fundamentals, Fifth Edition, McGraw-Hill Education, International Edition. ISBN: 978-0-073-52954-7.

[24] Pillay, P., Krishnan R., 1989. Modeling, simulation, and analysis of permanent-magnet motor drives. Part II. The brushless DC motor drive. IEEE Transactions Industry Applications, *25*, pp. 274-279.

[25] Millman, J., 1986. Microelectronics: Digital and Analog Circuits and Systems. McGraw-Hill Inc., US. ISBN: 978-0-070-42330-5.

[26] Saravana Perumaal, S., and Jawahar, N., 2013. Automated trajectory planner of industrial robot pick-and-place task. Int. Journal of Advanced Robotic Systems, *10*, pp. 1-17.

[27] Gosselin, C., and Angeles, J., 1990. Singularity analysis of closed-loop kinematic chains. IEEE Transactions On Robotics And Automation, *6*(3), pp. 281-290.

[28] Conconi, M., and Carricato, M., 2009. A new assessment of singularities of parallel kinematic chains. IEEE Transactions on Robotics, *25*(4), pp. 757-770.

[29] Project RobEcolo. URL http://robecolo.irccyn.ec-nantes.fr/

[30] Kaci, L., Briot, S., Boudaud, C., and Martinet, P., 2018. Design of a Wooden Five-bar Mechanism. Proceedings of the 22nd CISM-IFToMM Symposium on Robot Design, Dynamics, and Control (ROMANSY 2018), June 25-28, 2018, Rennes, France.

[31] Siemens, The performance-optimized and easy-to-use servo drive system, SINAMICS V90 datasheet.